Guided ion beam and theoretical study of the reactions of Au+ with H2, D2, and HD

Fengxia Li, Christopher S. Hinton, Murat Citir, Fuyi Liu, and P. B. Armentrout

Citation: J. Chem. Phys. **134**, 024310 (2011); doi: 10.1063/1.3514899
View online: http://dx.doi.org/10.1063/1.3514899
View Table of Contents: http://jcp.aip.org/resource/1/JCPSA6/v134/i2
Published by the American Institute of Physics.

Guided ion beam and theoretical study of the reactions of Au^+ with H_2, D_2, and HD

Fengxia Li,[a] Christopher S. Hinton, Murat Citir, Fuyi Liu,[b] and P. B. Armentrout[c]
Chemistry Department, University of Utah, 315 S. 1400 E. Rm 2020, Salt Lake City, Utah 84112, USA

(Received 27 September 2010; accepted 21 October 2010; published online 12 January 2011)

Reactions of the late third-row transition metal cation Au^+ with H_2, D_2, and HD are examined using guided ion beam tandem mass spectrometry. A flow tube ion source produces Au^+ in its ^1S ($5d^{10}$) electronic ground state level. Corresponding state-specific reaction cross sections for forming AuH^+ and AuD^+ as a function of kinetic energy are obtained and analyzed to give a 0 K bond dissociation energy of $D_0(Au^+–H) = 2.13 \pm 0.11$ eV. Quantum chemical calculations at the B3LYP/HW+/6-311+G(3p) and B3LYP/Def2TZVPP levels performed here show good agreement with the experimental bond energy. Theory also provides the electronic structures of these species and the reactive potential energy surfaces. We also compare this third-row transition metal system with previous results for analogous reactions of the first-row and second-row congeners, Cu^+ and Ag^+. We find that Au^+ has a stronger $M^+–H$ bond, which can be explained by the lanthanide contraction and relativistic effects that alter the relative size of the valence *s* and *d* orbitals. Results from reactions with HD provide insight into the reaction mechanism and indicate that ground state Au^+ reacts largely via a direct mechanism, in concordance with the behavior of the lighter group 11 metal ions, but includes more statistical behavior than these metals as well. © *2011 American Institute of Physics*. [doi:10.1063/1.3514899]

I. INTRODUCTION

Gold nanoparticles have drawn considerable attention because of the potential use in catalysis. In particular, nanoscale gold is very active for oxidation of carbon monoxide[1–5] (a phenomenon also explored theoretically)[6–8] and hydrocarbons.[9] Recent studies also show that gold nanoparticles smaller than about 4 nm deposited on TiO_2 activate H_2, with the perimeter interfaces identified as the active sites.[10] Density functional calculations on such systems suggest that positively charged gold atoms are not active in H_2 activation.[11] Related gas phase studies include reactions of neutral and cationic gold clusters with O_2,[12–15] and oxidation of CO on oxidized gold cluster cations and anions.[16–19] Gas phase studies of atomic gold cations by Wilkins and coworkers found reactions at thermal energies with a number of aliphatic and aromatic hydrocarbons using Fourier-transform ion cyclotron resonance spectrometry.[20,21] Under such conditions, Au^+ has also been shown to react with dimethyl peroxide to yield $Au^+(CH_2O)$, $AuCO^+$, as well as the dihydride AuH_2^+.[22] Previous work in our laboratory on reactions of atomic gold cations with O_2 and N_2O shows that the oxidation of gold is relatively inefficient, although the ^3D excited state can react at thermal energies with N_2O.[23] More pertinent to the present study is our study of the reaction of Au^+ with methane, which demonstrated that dehydrogenation to form $AuCH_2^+$ occurs in an activated reaction.[24] For most atomic transition metal cations, this process would be initiated by insertion of the metal into a C–H bond; however, with Au^+, direct H–H coupling from the methane in the presence of the metal ion was found to be the only low energy pathway found theoretically. Higher energies were required for C–H bond activation by oxidative addition to the metal center to form $AuH^+ + CH_3$ and $AuCH_3^+ + H$ products.

The activation of covalent bonds is an important process in many homogeneous and heterogeneous catalytic reactions.[25,26] To investigate this process in the absence of competing processes, the present work examines the activation of dihydrogen. The periodic trends in this chemistry are particularly interesting.[27–30] and there are now numerous experimental studies of the reactions of the ions of atomic first-row transition metals,[31–41] second-row transition metals,[39,40,42,44] third-row transition metals,[42,45,48] and other metals,[49–53] with dihydrogen, reaction (1), and its isotopic analogs, HD and D_2

$$M^+ + H_2 \rightarrow MH^+ + H. \quad (1)$$

The guided ion beam methods used in our laboratory can examine such reactions at hyperthermal energies, and thereby have the ability to investigate endothermic reactions and provide the bond dissociation energies (BDEs) for $M^+–H$ by analysis of the kinetic energy dependence of reaction (1).[30,54–57] We also investigate reactions of Au^+ with HD over a wide range kinetic energies, as such reactions have been shown to provide useful mechanistic information.[27,28,37,40,42–44] Finally, we compare the reactivities and mechanisms of Au^+ reacting with dihydrogen to those of its first-row and second-row congeners, Cu^+ and Ag^+.[41,43]

[a]Present address: Covance Laboratories Inc., Madison, Wisconsin 53704, USA.
[b]Present address: National Synchrotron Radiation Laboratory, University of Science and Technology of China, Hefei, China.
[c]Author to whom correspondence should be addressed. Electronic mail: armentrout@chem.utah.edu.

Another important aspect of such small systems is that they are amenable to detailed theoretical calculations that can be compared with the experimental results. Here, theoretical calculations on the AuH^+ and AuH_2^+ species are performed to assign electronic structures and explore the potential energy surfaces (PESs) for reaction. These are compared to previous theoretical results for AuH^+.[58–62]

II. EXPERIMENTAL AND THEORETICAL SECTION

A. Instrumentation

The guided ion beam tandem mass spectrometer on which these experiments were performed has been described in detail previously.[63] Briefly, reactant ions are generated in a direct current discharge flow tube (DC/FT) source described below. The ions are extracted from the source, accelerated, and focused into a magnetic sector momentum analyzer for mass selection of the primary reactant ions. Mass-selected ions are decelerated to a desired kinetic energy and focused into an octopole ion beam guide,[64,65] which uses radio-frequency electric fields to trap the ions in the radial direction and ensure complete collection of reactant and product ions. The octopole passes through a static gas cell that contains the reaction partner (here H_2, D_2, and HD) at a low pressure (usually ≤ 0.3 mTorr) so that multiple ion–molecule collisions are improbable. All products reported here result from single bimolecular encounters, as verified by pressure dependence studies. Product and unreacted primary ions drift to the end of the octopole where they are extracted, focused, passed through a quadrupole mass filter for mass analysis, and detected with a secondary electron scintillation ion detector using standard pulse counting techniques. Ion intensities are converted to absolute cross sections after correcting for background signals.[66] Absolute uncertainties in cross section magnitudes are estimated to be $\pm 20\%$.

The kinetic energy dependence of the ions is varied in the laboratory frame by scanning the dc bias on the octopole with respect to the potential of the ion source region. Ion kinetic energies in the laboratory frame, E_{lab}, are converted to energies in the center-of-mass frame, E_{CM}, using the formula $E_{CM} = E_{lab}\, m/(m + M)$, where m and M are the neutral and ionic reactant masses, respectively. All energies reported below are in the CM frame unless otherwise noted. Two effects broaden the cross section data: the thermal motion of the neutral reactant gas (Doppler broadening)[67] and the kinetic energy distribution of the reactant ion. The absolute zero and distribution of the ion kinetic energies are determined using the octopole beam guide as a retarding potential analyzer as described previously.[66] The distribution of ion kinetic energies is nearly Gaussian and has a typical full width at half-maximum between 0.3 and 1.0 eV (lab) in these studies. The uncertainty in the absolute energy scale is ± 0.05 eV (lab).

B. Ion source

Atomic gold metal cations are formed in a DC/FT source.[68] This source consists of a cathode held at high negative voltage (0.7–1.8 kV) over which a flow of approximately 90% He and 10% Ar passes at a total pressure of 0.3–0.5 Torr and ambient temperature. The cathode in this work is gold-plated aluminum or gold foil held on an iron cylinder. Ar^+ ions created in the discharge are accelerated toward the metal cathode, thereby sputtering Au^+ ions. These ions are then swept down a 1 m long flow tube. The flow conditions used in this ion source provide about 10^5 thermalizing collisions between an ion and He ($\sim 10^4$ collisions with Ar) before the ions enter the guided ion beam apparatus. As discussed in previous papers,[23,24] excited states of Au^+ are observed to survive these flow conditions, although the population of these states varies appreciably, suggesting that small amounts of contaminant gases can effectively quench them. Complete quenching of all excited states can be achieved by the addition of N_2O as a cooling gas.[23]

C. Data analysis

The kinetic energy dependence of product cross sections is analyzed to determine E_0, the energy threshold for product formation at 0 K. E_0 differs from the apparent threshold observed under laboratory conditions because of the kinetic and internal energy distributions of the reactants. These contributions allow reactions to occur at energies below E_0. To determine E_0, endothermic reaction cross sections are modeled using Eq. (2),[55,56,69–71]

$$\sigma(E) = \sigma_0 \sum g_i (E + E_i + E_{el} - E_0)^n / E, \qquad (2)$$

where σ_0 is an energy-independent scaling factor E is the relative kinetic energy of the reactants, E_{el} is the electronic energy of the Au^+ reactant, and n is an adjustable parameter. When the N_2O quenching gas is used in the source, the Au^+ reactant is in its ^1S ground state such that $E_{el} = 0.0$ eV. Equation (2) includes an explicit sum of contributions from rovibrational states of reactants at 300 K, denoted by i, having energies E_i and populations g_i, where $\sum g_i = 1$. The vibrational frequencies and rotational constants used to determine E_i in this work are taken from the literature for H_2 and D_2.[72] Before comparison with the experimental data, Eq. (2) is convoluted with the kinetic energy distributions of the ions and neutral reactants at 300 K. The σ_0, n, and E_0 parameters are then optimized using a nonlinear least-squares analysis to give the best reproduction of the data.[55,56,70,71] Error limits for E_0 are calculated from the range of threshold values for different data sets over a range of acceptable n values combined with the absolute uncertainty in the kinetic energy scale.

D. Theoretical calculations

Quantum chemistry calculations reported here are performed with the GAUSSIAN 03 suite of programs.[73] In all cases, the thermochemistry calculated and cited here is corrected for zero point energy effects without scaling the frequencies. In previous work,[23] we considered several combinations of theoretical approaches and basis sets and compared the results to five experimental properties of gold and its molecules. (1) The $^1S - {}^3D$ excitation energy of Au^+, $E_{ex}(Au^+) = 2.288$ eV for the statistical average of all

spin-orbit energies for the ^3D_J levels.[74] (2) The ionization energy of Au, IE(Au) = 9.22553 eV.[75] (3) The 0 K bond energy of AuO, D_0(Au–O) = 2.27 ± 0.22 eV.[76,77] (4) The 0 K bond energy of $AuCH_2^+$, $D_0(Au^+–CH_2) = 3.70 \pm 0.07$ eV.[24] (5) A preliminary value for the 0 K bond energy of AuH^+, $D_0(Au^+–H) = 2.17 \pm 0.08$ eV.[23,24] Theoretical approaches considered included the B3LYP hybrid density functional method,[78,79] and the CCSD(T,full) approach. Four basis sets for Au were considered, all of which retain 19 explicit electrons. Ohanessian *et al.*[58] describe a basis set that is based on the small core (60 electron) relativistic effective core potential (ECP) and valence basis set of Hay–Wadt (HW),[80] equivalent to the Los Alamos ECP (LANL2DZ) basis set. Whereas the HW–ECP is optimized for neutral atoms, the altered basis set of Ohanessian *et al.* (designated here as HW+) accounts for differential contraction of the *s* orbitals compared to the *d* orbitals induced by the positive charge. We also considered the Stuttgart–Dresden relativistic small core ECP basis set of Dolg *et al.*[81] (SDD); the SBKJC VDZ ECP basis set (SBKJC, also known as CEP-121G);[82] and the Def2TZVPP basis set,[83] a balanced set of triple zeta quality + polarization functions that also uses the SDD ECP for Au. The SBKJC basis set was augmented with one *f* polarization function (exponent = 0.89) and *s* and *p* diffuse functions (both exponents = 0.01) as per Varganov *et al.*[84] (designated here as SBKJC*). For the HW+, SDD, and SBKJC* basis sets on Au, calculations use a large basis set for the other elements, triple zeta with diffuse and polarization functions, 6-311++G(3df,3p). This basis set gives good results for the thermochemistry of dihydrogen, with deviations from experiment of less than 0.03 eV for the 0 K bond energy of H–H (4.505 eV calculated vs 4.478 eV experimental).[72] Def2TZVPP basis set calculations use this basis set on all elements. The comparison of all of these combinations with the experimental data indicates that the overall best reproduction is achieved using the B3LYP/Def2TZVPP and B3LYP/SBKJC* combinations, with the CCSD(T)/Def2TZVPP combination being only slightly worse and better than any other CCSD(T)/basis set combination.[23]

The most appropriate choice for a level of theory to calculate covalent metal ligand bond energies has been investigated for the first and third row transition metal methyl cations by Holthausen *et al.*[85] In this study, B3LYP, Beck-Half-and-Half-LYP (BHLYP), and QCISD(T) methods were considered with a basis set consisting of a polarized double-zeta basis on C and H and the Hay–Wadt relativistic ECP with valence electrons added. The symmetries of the metal methyl species were constrained to C_{3v}. For the first row MCH_3^+ species (M = Sc – Cu), where experimental results are available for all metals,[54] these authors conclude that the B3LYP functional overbinds, with a mean absolute deviation (MAD) from experiment of 0.41 eV. The BHLYP functional and the QCISD(T) methods perform more accurately, with MADs of 0.18 and 0.20 eV, respectively. For the third row elements, the bond energies calculated using B3LYP were again higher than those for BHLYP and QCISD(T). On the basis of these results, the present study includes calculations for the various product ions using the B3LYP and BHLYP functionals with both the HW+/6-311++G(3df,3p) and Def2TZVPP basis sets, along with QCISD(T) and CCSD(T,full) calculations. Such calculations will be explicitly noted, but unless otherwise designated, our results will refer to a B3LYP/HW+/6-311+G(3p) level of theory. For AuH_2^+ species where multiple bonds to Au^+ are formed, this level of theory is the only one applied.

At all levels of theory, the ground state for Au^+ is a ^1S state. Excitation energies to the lowest lying triplet state, ^3D, are calculated to be 2.361 eV (B3LYP/HW+), 2.271 eV (B3LYP/Def2TZVPP), 2.473 eV (CCSD(T,full)/HW+), and 2.411 eV (CCSD(T,full)/Def2TZVPP, showing that the atomic excitations are not strongly dependent on the choices made. These calculated triplet excitation energies can be favorably compared to the experimental value of 2.288 eV (statistically weighted mean of all spin-orbit levels).[74]

III. EXPERIMENTAL RESULTS

A. Reactions of Au^+ with H_2 and D_2

Figures 1 and 2 show cross sections as a function of kinetic energy for the bimolecular reaction of H_2 and D_2 with Au^+ produced in the DC/FT source with N_2O added to quench residual excited states. Reaction (1) and its deuterated analog are the only processes observed. The energy dependences of the cross sections for the two systems are quite consistent, although the absolute magnitudes of the $Au^+ + H_2$ and $Au^+ + D_2$ reaction cross sections differ by about 20%, comparable to the estimated 20% experimental uncertainty. Data taken for the D_2 system were taken upon two occasions (separated by 6 years) and yielded identical energy dependences, but magnitudes differing by about 30%, again comparable to the estimated uncertainty. Both cross sections rise from apparent thresholds near 2.0 eV and reach maxima near the dissociation energy of H_2, $D_0(H_2) = 4.478$ eV, or D_2,

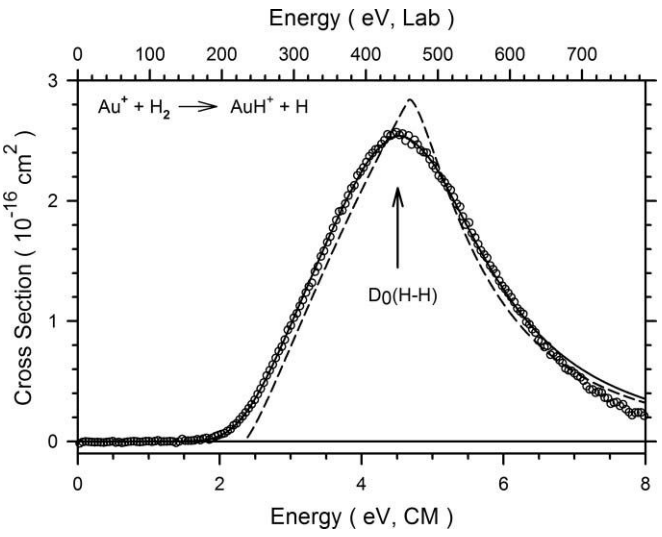

FIG. 1. Cross sections for reaction of Au^+ (^1S) with H_2 as a function of kinetic energy in the center-of-mass frame (lower axis) and laboratory frame (upper axis). The model of Eq. (2) with parameters from Table I is shown as a dashed line. The solid line shows this model convoluted over the kinetic and internal energy distributions of the reactant neutral and ion. The arrow indicates D_0 (H–H) at 4.478 eV.

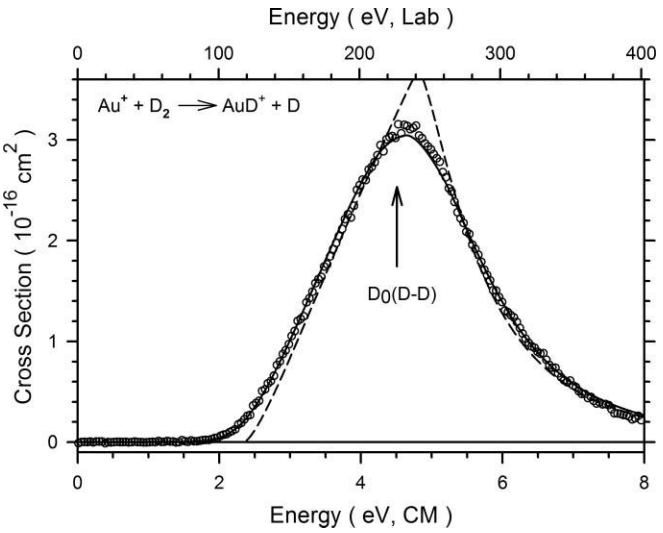

FIG. 2. Cross sections for reaction of Au^+ (^1S) with D_2 as a function of kinetic energy in the center-of-mass frame (lower axis) and laboratory frame (upper axis). The model of Eq. (2) with parameters from Table I is shown as a dashed line. The solid line shows this model convoluted over the kinetic and internal energy distributions of the reactant neutral and ion. The arrow indicates D_0 (D−D) at 4.556 eV.

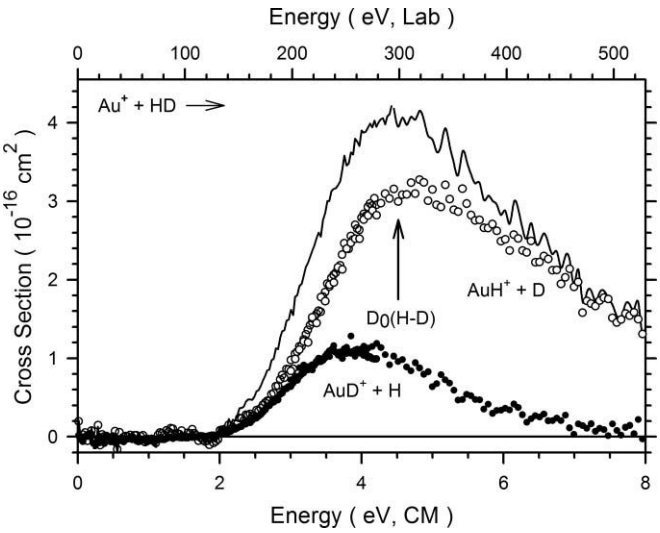

FIG. 3. Cross sections for reaction of Au^+ (^1S) with HD as a function of kinetic energy in the center-of-mass frame (lower axis) and laboratory frame (upper axis). The arrow indicates D_0(H−D) at 4.514 eV.

$D_0(D_2) = 4.556$ eV.[72] At higher energies, the $AuH^+(AuD^+)$ products can be formed with internal energies in excess of the bond dissociation energy, such that these products begin to dissociate in the overall reaction (3)

$$Au^+ + H_2(D_2) \rightarrow AuH^+(AuD^+) + H(D) \rightarrow Au^+ + 2H(D). \quad (3)$$

The observation that the experimental cross sections reach maxima very close to the H_2 (D_2) bond energies illustrates that process 3 begins promptly at its thermodynamic threshold.

B. Reactions of Au^+ with HD

Au^+ reacts with HD to yield both AuH^+ and AuD^+ in reactions (4) and (5) (Fig. 3)

$$M^+ + HD \rightarrow MH^+ + D, \quad (4)$$

$$\rightarrow MD^+ + H. \quad (5)$$

Because of the close proximity of the product masses, there can easily be some overlap between these signals depending on the mass resolution used in the quadrupole mass filter. In the present system, it was carefully checked that high resolution leading to separation of these products could be used without sacrificing efficient collection of the product ions. The accuracy of the final results is confirmed by reasonable agreement between the magnitudes of the total cross sections for the HD system, which matches the most recent data taken for the D_2 system.

The total cross section in the HD system exhibits endothermic behavior and rises from an apparent threshold that is comparable to those of the H_2 and D_2 systems. The total cross section reaches a maximum near the bond dissociation energy of HD, 4.51 eV.[72] The individual AuH^+ and AuD^+ cross sections behave differently. Although thresholds of both channels are similar, the energy at which the AuD^+ cross section reaches its maximum is lower than that for AuH^+, which is comparable to those of reaction (1) and its fully deuterated analog. In the HD system, the AuD^+ cross section begins to decline at an energy before the onset of dissociation in the analog of reaction (3) because of competition with the AuH^+ + D channel. Furthermore, the AuD^+ cross section declines more rapidly than the AuH^+ cross section as the energy increases further. The relative high-energy behavior shows that the D atom carries away more energy from AuH^+ than the H atom carries away from AuD^+. This effect is typical of atomic ion reactions with H_2, HD, and D_2,[28,40,42–44] and has been discussed in detail elsewhere.[28,86–88]

IV. THERMOCHEMICAL AND THEORETICAL RESULTS

A. Thermochemistry

The endothermic cross sections in the H_2 and D_2 reaction systems are analyzed in detail using Eq. (2). Typical models are shown in Figs. 1 and 2 and can be seen to reproduce the experimental results very well until about 7 eV. At energies above $D_0(H_2)$ and $D_0(D_2)$, where reaction (3) can begin, the analyses include a model for this subsequent dissociation, as outlined in detail elsewhere.[89] This high energy model requires two parameters: E_D is the onset for AuH^+ (AuD^+) dissociation in reaction (3), and the exponent p determines the energy dependence, similar to n in Eq. (2). For the results shown in Figs. 1 and 2, E_D is fixed close to the H_2 (D_2) bond energy and the optimum value of p was found to be 3.

The optimum values of the parameters in Eq. (2) for these systems are listed in Table I. These values represent the average of five data sets for each system. As can be seen in Figs. 1 and 2, the optimum values of E_0 differ appreciably from the apparent thresholds, which is largely a result of the large velocity distribution of the light H_2 (D_2) reactant. Be-

TABLE I. Parameters of Eq. (2) used in modeling reaction (1) and the resultant bond energies.

Reaction	σ_0	n	E_0 (eV)	$D_0(Au^+-H)$ (eV)
$Au^+ + H_2$	4.3 ± 0.6	1.4 ± 0.2	2.32 ± 0.07	2.16 ± 0.07
$Au^+ + D_2$	5.0 ± 0.7	1.3 ± 0.2	2.43 ± 0.09	2.09 ± 0.09[a]

[a]Value corrected for the zero point energy difference of 0.039 eV. See text.

cause the convoluted form of Eq. (2) includes all sources of energy (rotational, vibrational, translational, and electronic energy distributions of reactants are explicitly included in the modeling), the E_0 threshold energies determined correspond to 0 K values. From the thresholds measured, the BDEs for the metal-ligand cations observed in reaction (1) can be calculated using Eq. (6) and an analogous equation for the deuterated system

$$D_0(Au^+-H) = D_0(H-H) - E_0, \quad (6)$$

where $D_0(H–H) = 4.478$ eV and $D_0(D–D) = 4.556$ eV.[72] This equation assumes that there is no activation barrier in excess of the endothermicity of the reaction, an assumption that is often true for ion-molecule reactions because of the long-range attractive forces[71] and one that can be tested using theory; see below.

A summary of the Au^+–H bond energies derived from the present experiments with both H_2 and D_2 is given in Table I. This includes adjusting the value for $D_0(Au^+–D)$ for the zero point energy difference between AuD^+ and AuH^+. This correction uses a vibrational frequency of 2173 cm^{-1} for AuH^+ and 1542 cm^{-1} for AuD^+ as calculated here for the $^2\Sigma^+$ state (Table II), a value for AuH^+ in reasonable agreement with 2274 cm^{-1} calculated by Ohanessian *et al.*,[58] 2187 cm^{-1} calculated by Schwerdtfeger *et al.*,[59] and 2364 cm^{-1} calculated by Kaldor and Hess.[61] Thus the zero point energy difference in the AuH^+ and AuD^+ bond energies is 0.039 ± 0.004 eV, assuming a 10% uncertainty in the frequency. The Au^+–H bond energies obtained from the H_2 and D_2 systems are in good agreement with one another (Table I). Our best value for this bond energy is the weighted average of these two values, 2.13 ± 0.11 eV (206 ± 11 kJ/mol), where the uncertainty is two standard deviations of the mean.

TABLE II. Theoretical geometries and energies for AuH^+.[a]

State	$r_e(Au-H)$ (Å)	Frequency (cm^{-1})	E_{rel} (eV)[b]	D_0 (eV)
$^2\Sigma^+$	1.553	2173	0.0	2.08
	1.542	*2194*	*0.0*	*2.08*
	1.523	**2263**	**0.0**	**1.90**
$^2\Delta$	1.594	2103	1.641	0.43
	1.590	*2064*	*1.681*	*0.40*
	1.574	**2118**	**1.735**	**0.17**
$^2\Pi$	1.651	1955	2.126	–0.06
	1.641	*1940*	*2.088*	*–0.01*
	1.628	**1979**	**2.120**	**–0.21**

[a]Results of B3LYP/HW+/6-311+G(3p) (roman), B3LYP/Def2TZVPP (italic), and CCSD(T,full)/Def2TZVPP (bold) calculations.
[b]Energies relative to the ground state including zero point energies (unscaled).

It can also be noted that AuH^+ bond energies were determined in our study of the reactions of Au^+ with CH_4 and CD_4,[24] where values of 1.94 ± 0.08 and 1.89 ± 0.08 eV, respectively, were obtained (after zero point energy correction in the latter case). In these systems, the dominant low energy processes are dehydrogenation to form $AuCH_2^+ + H_2$ ($AuCD_2^+ + D_2$), such that competition with this channel can elevate the thresholds for $AuH^+ + CH_3$ ($AuD^+ + CD_3$). Therefore, these bond energies are conservatively viewed as lower limits, consistent with the present results.

B. AuH^+ electronic structure

Generalized valence bond (GVB) calculations indicate that AuH^+ has a $^2\Sigma^+$ ground state with a covalent bond formed between a *sd* hybridized (30% 6*s* and 70% 5*d*) orbital on Au^+ (^1S) and the 1*s* orbital on H.[58] Formation of this bond requires mixing of the ^1S ($5d^{10}$) ground state of Au^+ with the excited ^3D ($6s^15d^9$) state. GVB theory followed by correlation consistent configuration interaction calculations provides a 0 K BDE for AuH^+ of 1.45 eV for the $^2\Sigma^+$ ground state.[58] Schwerdtfeger *et al.* determined a value of 1.83 eV using a coupled electron pair approximation method.[59] Ishikawa *et al.* calculated a D_e of 0.59 eV for the ground $\Gamma_{1/2}$ state using a fully relativistic Dirac–Fock SCF treatment.[60] Kaldor and Hess performed a relativistic coupled cluster calculation to find D_e as 1.97 eV,[61] as also reported by Hrušák *et al.*[62] Overall, these values are lower than our experimental value of 2.13 ± 0.11 eV.

Our calculations find BDEs of 2.08 / 1.99 / 2.00 / 2.08 eV when using the B3LYP functional and the HW+/SDD/SBKJC*/Def2TZVPP basis sets. At the BHLYP level, the BDEs are 1.66 / 1.43 / 1.61 / 1.68 eV and at the CCSD(T,full) level, which are the same as QCISD(T) results, the BDEs are 1.66 / 1.26 / 1.84 / 1.90 eV. As found by Holthausen *et al.* for the third-row transition metal ion methyl cations,[85] the B3LYP functional generally overbinds compared to the BHLYP and QCISD(T) methods; however, the B3LYP/HW+ and B3LYP/Def2TZVPP calculations are in good agreement with our experimental result in this system and the CCSD(T,full)/Def2TZVPP result is only slightly too low. It can also be noted that BLYP/SBKJC* and BP86/SBKJC* calculations, which were checked because of recommendations by Wu (who used the SBKJC basis set without additional polarization functions),[90] yield BDEs of 2.22 and 2.38 eV, respectively. These values are slightly higher than experiment, consistent with results for the other calibration values, $D_0(AuO)$ and $D_0(AuCH_2^+)$.[23] Bond lengths for AuH^+ calculated here include 1.553 Å (B3LYP/HW+), 1.547 Å (BHLYP/HW+), 1.542 Å (B3LYP/Def2TZVPP), 1.536 Å (BHLYP/Def2TZVPP), and 1.523 Å (CCSD(T)/Def2TZVPP). These values are in good agreement with those calculated by Ohanessian *et al.*, 1.539 Å,[58] Schwerdtfeger *et al.*, 1.513 Å,[59] Ishikawa *et al.*,[60] 1.56 Å, and Kaldor and Hess, 1.514 Å.[61]

The $^2\Sigma^+$ ground state has a valence electronic configuration of $1\sigma_b^2 2\sigma^1 1\pi^4 1\delta^4$, where σ_b represents the bonding orbital and the remaining are nonbonding orbitals on the

metal with the 2σ being largely $6s$. We also found two excited states, $^2\Delta$ and $^2\Pi$, having valence electronic configurations of $1\sigma_b{}^2 2\sigma^2 1\pi^4 1\delta^3$ and $1\sigma_b{}^2 2\sigma^2 1\pi^3 1\delta^4$, respectively. As summarized in Table II, these states have longer bond lengths than the $^2\Sigma^+$ ground state by 0.04–0.05 and ~0.1 Å, respectively, with excitation energies of 1.64–1.74 and 2.09–2.13 eV, respectively.

C. AuH_2^+ states

To explore coarse features of the potential energy surface for reaction (1), we also calculated the properties of AuH_2^+ complexes at the B3LYP/HW+/6-311+G(3p) level. We considered the reaction of H_2 with both the ^1S ($5d^{10}$) ground state and ^3D ($5d^9 6s^1$) excited state of Au^+ for perpendicular (C_{2v} symmetry) and collinear reaction pathways. In both cases, the z axis is defined as the symmetry axis, with the molecule lying in the xz plane. Results for stable singlet and triplet states of AuH_2^+ and related transition states are summarized in Table III. The complete surfaces for the various AuH_2^+ states in C_{2v} symmetry as a function of bond angle are shown in Fig. 4. These were obtained from relaxed PES scan calculations starting at the optimized geometry of each state.

On the singlet surface in C_{2v} symmetry, our calculations find a $^1A_1$ ground state of AuH_2^+ with a 0 K BDE of 0.87 eV relative to the Au^+ (^1S) + H_2 asymptote. The geometry of the AuH_2^+ ($^1A_1$) ground state corresponds to an intact dihydrogen molecule bound to Au^+. This is identified by long Au^+–H bond lengths of 1.787 Å, a small HAuH bond angle of 27.4°, and a short H–H bond length of 0.847 Å, slightly longer than that calculated for free H_2, 0.743 Å. Another minimum corresponding to an inserted species is found along the $^1A_1$ surface at a HAuH bond angle of 75.7°. Now the Au^+–H bond lengths are shorter, 1.543 Å, but the well is only 0.65 eV deep. A transition state between these two minima is found at ∠HAuH = 52.5°, only 0.008 eV above the inserted minimum once zero point energies are included. Alternatively, the H_2 molecule in the AuH_2^+ ($^1A_1$) molecule can be rotated in the plane of the molecule. This gradually increases the energy leading to a linear $AuHH^+$ ($^1\Sigma^+$) transition state 0.42 eV higher in energy (but still bound by 0.45 eV; Table III).

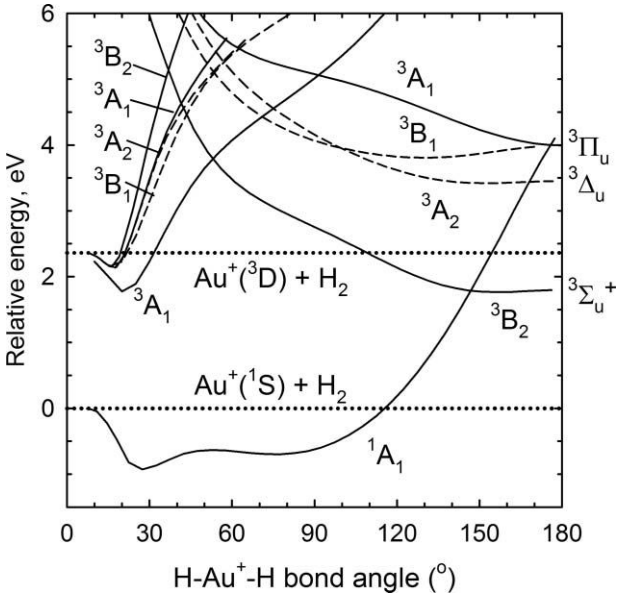

FIG. 4. B3LYP/HW+/6-311+G(3p) calculations of the potential energy surfaces for the interaction of Au^+ with H_2 in C_{2v} symmetry as a function of the H–Au^+–H bond angle in degrees. Surfaces with A_1 and B_2 (A′) symmetry are shown by full lines, with B_1 and A_2 (A″) surfaces shown by dashed lines. Dotted lines indicate the experimental energy zero, corresponding to the Au^+(^1S) + H_2 ground state, and the theoretical energy for the Au^+(^3D) + H_2 excited state.

TABLE III. Theoretical geometries, energies, and vibrational frequencies for AuH_2^+.[a]

State	r_e(Au–H) (Å)	r_e(H–H) (Å)	∠HAuH (°)	E_{rel} (eV)[b]	ν (cm^{-1})
$^1A_1$	1.787 (2)	0.847	27.4	–0.871	883, 1329, 3090
$^1A_1$	1.543 (2)	1.893	75.7	-0.651	662, 2230, 2286
$^1A_1$	1.576 (2)	1.393	52.5	-0.643	–775, 2088, 2171
$^1\Sigma^+$	1.843, 2.616	0.773	0.0	–0.446	–643(2), 718, 3919
$^3\Sigma_u{}^+$	1.703 (2)	3.406	180.0	1.692	–412(2), 1031, 1671
$^3B_2$	1.680 (2)	3.287	156.2	1.708	502, 1296, 1718
$^3\Sigma^+$	1.894, 2.698	0.804	0.0	1.758	191(2), 714, 3249
$^3A'$	1.988, 2.435	0.788	17.0	1.744	196, 696, 3675
$^3A_1$	2.168 (2)	0.781	20.8	1.744	–347, 562, 3878
$^3\Delta$	2.180, 2.943	0.763	0.0	2.133	29(2), 367, 3997
$^3A_1$	2.512 (2)	0.759	17.4	2.146	–166, 398, 4153
$^3A_2$	2.510 (2)	0.759	17.4	2.146	–183, 400, 4152
$^3A''$	2.248, 2.790	0.762	12.3	2.149	209, 443, 4066
$^3B_2$	2.643 (2)	0.756	16.4	2.166	–206, 308, 4202
$^3\Pi$	2.328, 3.084	0.756	0.0	2.178	–90, 73, 320, 4131
$^3B_1$	2.595 (2)	0.757	16.8	2.180	336, 423, 4180
$^3\Delta_u$	1.722 (2)	3.444	180.0	3.350	–342(2), 1093, 1680
$^3A_2$	1.701 (2)	3.299	151.8	3.358	421, 1315, 1716
$^3B_1$	1.714 (2)	3.106	129.9	3.763	461, 1604, 1665
$^3\Pi_u$	1.770 (2)	3.540	180.0	3.914	–478, 581, 994, 1557

[a]Calculations using B3LYP/HW+/6-311+G(3p). Degeneracies in parentheses.
[b]Energies relative to Au^+(^1S) + H_2 (–136.263792 E_h) including zero point energies (unscaled).

On the triplet surface, approach of $Au^+(^3D)$ to H_2 in C_{2v} symmetry yields five states ($^3A_1$, $^3B_1$, $^3A_2$, $^3A_1$, $^3B_2$) corresponding to having the electron hole in the 5*d* orbitals in the $a_1(dz^2)$, $b_1(dyz)$, $a_2(dxy)$, $a_1(dx^2\text{-}y^2)$, and $b_2(dxz)$, respectively. The lower-lying $^3A_1$ has a bond energy relative to the reactant asymptote of 0.62 eV, whereas the other four states have shallower minima bound by 0.22 ($^3A_1$,$^3A_2$), 0.20 ($^3B_2$), and 0.18 ($^3B_1$) eV. In all cases, these states have H_2 loosely bound to Au^+ with long Au^+–H bond lengths, between 2.17 and 2.64 Å, small HAuH bond angles between 16° and 21°, and short H–H distances of 0.75–0.78 Å (Table III). Notably, for all but the $^3B_1$ state, these species have imaginary frequencies in the asymmetric stretch (or equivalently, rotation of H_2), such that they will all collapse to other geometries. This conversion was explicitly examined for the low-lying $^3A_1$ state where rotation of the H_2 molecule leads to a minimum having C_s symmetry, $^3A'$, but an energy including zero point corrections that is the same as the C_{2v} transition state. Further rotation leads to the linear $Au^+(HH)$ $^3\Sigma^+$ state bound by 0.60 eV relative to the reactant asymptote, such that full rotation of the H_2 moiety in the AuH_2^+ plane requires only 0.014 eV. A similar situation occurs for the other states leading to $^3\Delta$ and $^3\Pi$ states, which lie 0.38 and 0.42 eV above the $^3\Sigma^+$ state (Table III). In this case, the $^3\Delta$ is a stable minimum whereas the $^3\Pi$ state has an imaginary frequency associated with H_2 rotation in one plane. For both of these linear states, rotation of the H_2 will lead to an A′ and an A″ state, of which only the $^3A''$ state evolving from the $^3\Delta$ was located (and leads to the $^3A_2$ state in C_{2v} symmetry). Note that a collinear orientation between Au^+ and H_2 is qualitatively favorable for the triplet surface as the single 6*s* electron on Au^+ (^3D) makes it similar to H (^2S), which is known to react most efficiently with H_2 along a collinear $C_{\infty v}$ path, rather than a perpendicular C_{2v} path. Relaxed PES scans show that the collinear pathway is a viable reaction pathway with approach of Au^+ (^3D) to H_2 being attractive and leading to $AuHH^+$ ($^3\Sigma^+$, $^3\Pi$, and $^3\Delta$).

Several triplet states corresponding to covalently bound dihydrides were also located. These all have Au–H bond lengths between 1.68 and 1.77 Å and bond angles of 130°–180° (Table III). Of these, the one having the lowest energy is $^3B_2$, which has an HAuH bond angle of 156.2°, short AuH bond lengths (1.68 Å), and a long H–H bond distance (3.29 Å). Bending the molecule through its linear form requires little energy, such that the $^3\Sigma_u^+$ transition state actually lies lower in energy (by 0.02 eV) once zero point corrections are included. The electronic configuration of this state has a hole in the $a_1(5dx^2\text{-}y^2)$ orbital, which now lies mostly parallel with the HAuH molecule along the x axis, and the highest occupied molecular orbital is a b_2 orbital that is largely 6*p*x. As the electron hole in the 5*d* orbitals is moved, $^3A_2$ (b_1 hole), $^3B_1$ (a_2 hole), and $^3A_1$ (b_2 hole) states are also generated, but lie 1.65–2.21 eV higher in energy. At HAuH bond angles of 180°, the $^3A_2$ state becomes a $^3\Delta_u$ state degenerate with another $^3B_2$ state, and the $^3B_1$ and $^3A_1$ states become degenerate $^3\Pi_u$ states. Both the $^3\Delta_u$ and $^3\Pi_u$ states have imaginary frequencies such that they collapse to the appropriate C_{2v} states.

Because of the C_{2v} symmetry restriction, the PESs in Fig. 4 cannot examine the AuH^+ + H dissociation asymptote. It seems likely that these products can be formed from the AuH_2^+ intermediates with no barriers in excess of the endothermicity for the following reasons. The $^2\Sigma^+$ ground state of AuH^+ can interact with H(^2S) to form both a low-spin singlet state and a high-spin triplet state of AuH_2^+. Along the singlet surface, covalent coupling of the nonbonding 2σ electron of AuH^+ ($^2\Sigma^+$) with H (1s) occurs such that the surface should be strongly attractive, whereas no covalent bond formation is involved in formation of the high-spin state. To verify this hypothesis, we performed a relaxed PES scan at the B3LYP/HW+/6-311+G(3p) level starting with the $AuH_2^+(^1A_1)$ species and systematically lengthening the H–H bond. As this bond length increases, the bond angle, which starts at 27.4°, gradually opens to about 130° and leads directly to AuH^+ ($^2\Sigma^+$) + H (^2S) products with no barriers in excess of the endothermicity. Likewise, from either the singlet or triplet linear $AuHH^+$ adduct, lengthening the H–H bond leads to AuH^+ ($^2\Sigma^+$) + H products with no barrier.

V. DISCUSSION

The three group 11 metal ions, Cu^+, Ag^+, and Au^+, all have ^1S ground states with nd^{10} configurations, but despite this similarity, the reactivity with dihydrogen is distinct. The maximum cross sections for the three metal cations are 0.75×10^{-16} cm^2, 0.55×10^{-16} cm^2, and 3.2×10^{-16} cm^2, respectively.[41,43] Thus, the probability of the reaction for Au^+ is much larger than for the lighter congeners. This is partly because the BDEs are 0.92 ± 0.13, 0.41 ± 0.06, and 2.13 ± 0.11 eV, respectively,[41,43] such that the onset for the reaction with Au^+ occurs at much lower energy. Further comparison of the group 11 metal ions is facilitated by examining the reaction mechanisms as revealed by the reaction with HD.

Previous work on the first-row transition metal cations indicates that the product branching ratio in the reaction of M^+ with HD is very sensitive to the reaction mechanism.[27,28,40,43,44,71] and is governed by three "rules." (1) If M^+ has an electron configuration with empty 4*s* and 3*d*σ orbitals, such as for a $3d^n$ configuration where $n < 5$, the reaction is efficient and may proceed by an insertion mechanism. These processes are characterized by product branching ratio in the HD system, σ (MH^+ + D)/σ (MD^+ + H), that are near unity (or $\sigma_{MH}+/\sigma_{Total}$ values near 0.5 until product dissociation begins to occur), consistent with statistical behavior of a long-lived intermediate. (2) If either the 4*s* or 3*d*σ orbital is occupied and the M^+ state is low-spin, such as for $3d^n$ ($n > 5$) or low spin coupled $3d^{n-1}4s^1$ configurations, the reaction occurs efficiently via a direct mechanism. These processes are characterized by a product branching ratio in the HD system that favors MH^+ by a factor of 2–4 (or $\sigma_{MH}+/\sigma_{Total}$ ratios between 0.66 and 0.8), consistent with arguments concerning the conservation of angular momentum.[70,86,91–93] Because of zero point energy differences in the thresholds, which allow formation of MD^+ to occur at slightly lower energies than MH^+, the $\sigma_{MH}+/\sigma_{Total}$ ratios generally increase with energy from a starting point near 0.66–0.8. (3) If either the 4*s* or 3*d*σ orbital is occupied and the M^+ state has a high-spin coupled $3d^{n-1}4s^1$ configuration, the reaction is inefficient and tends to react impulsively. These processes are characterized by a

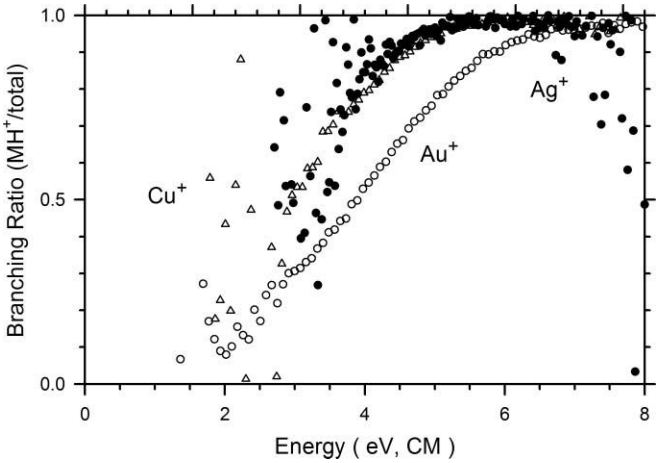

FIG. 5. Product branching fractions (σ_{MH+} / σ_{Total}) for reactions of Cu^+ (open triangles), Ag^+ (closed circles), and Au^+ (open circles) with HD as a function of kinetic energy in the center-of-mass frame.

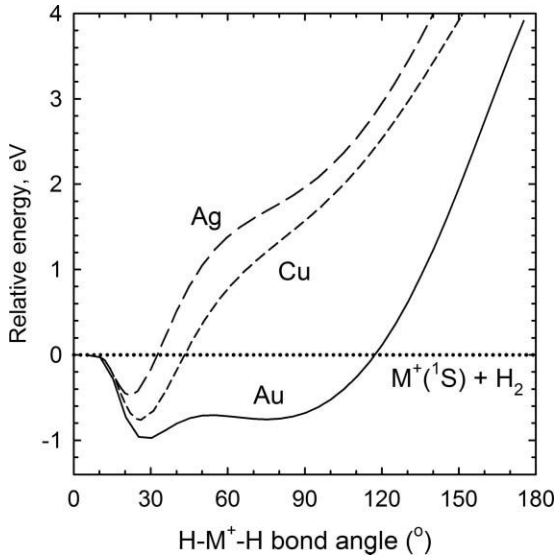

FIG. 6. B3LYP/Def2TZVPP calculations of the potential energy surfaces for the interaction of M^+ with H_2 in C_{2v} symmetry along the singlet surface as a function of the H−M^+−H bond angle in degrees for M = Au (solid), Ag (long dash), and Cu (short dash). The dotted line indicates the experimental energy zero, corresponding to the $M^+(^1S) + H_2$ ground state.

product branching ratio in the HD system that favors $MD^+ + H$ by a large factor (small values of the $\sigma_{MH}{}^+/\sigma_{Total}$ ratio) and exhibit shifts in the thresholds for the H_2 and D_2 systems versus the HD system. Note that these rules are only appropriate for the diabatic reaction behavior, i.e., cases where the electron configuration of the metal ions remains essentially static throughout the course of the reaction.

Results for the reactions of Cu^+, Ag^+, and Au^+ are compared in Fig. 5 in terms of the fraction of metal hydride ion product formed, $\sigma_{MH+}/\sigma_{Total}$. For all group 11 metal cations, the ground states have nd^{10} electron configurations such that these ions should react with dihydrogen in a direct process according to "rule 2."[41,43] The behavior exhibited by Cu^+ and Ag^+ are typical examples of such direct reactions with branching ratios having very similar energy dependences. Au^+ (^1S) falls into the same general category as its lighter congeners but the energy dependence is less abrupt and has a $\sigma_{MH+}/\sigma_{Total}$ ratio closer to 0.5 than the lighter congeners. This observation suggests that the gold system has more statistical pathways available to it, compared to copper and silver.

To understand this difference, we consider the perpendicular approach of M^+ and H_2 (C_{2v} symmetry). The most favorable interaction occurs when there is an acceptor orbital in the metal ion that interacts with the doubly occupied σ-bonding orbital of H_2 (having a_1 symmetry) and a donor orbital on the metal ion that interacts with the empty σ^*-antibonding orbital of H_2 (having b_2 symmetry). These interactions effectively weaken and lengthen the H_2 bond while simultaneously building electron density between the metal and H atoms. For the group 11 metal cations in their ^1S (d^{10}) ground state, M^+ has an empty valence s orbital that can act as the acceptor forming the a_1 bonding orbital of $MH_2{}^+$ by combining with the doubly occupied σ_g orbital on H_2. When the $b_2(dxz)$ orbital is doubly occupied, as it must be for the ^1S (d^{10}) state, there is also an attractive interaction that forms the b_2 bonding orbital of $AuH_2{}^+$ by combining with the unoccupied σ_u antibonding orbital of H_2. However, the double occupation in the $a_1(dz^2)$ and $a_1(dx^2\text{-}y^2)$ nonbonding orbitals lead to repulsive interactions with the occupied σ_g orbital on H_2, which reduces the bonding interaction compared to open shell transition metals. This repulsion can be relieved by *sd* hybridization, which effectively removes electron density from the $a_1(dz^2)$ orbital and leads to the $^1A_1$ inserted state of $MH_2{}^+$. For $AuH_2{}^+$, this state has a ∠HAuH bond angle of 76° (Table III), close to the 90° expected for a pure *sd* hybrid, and is only 0.22 eV above the global ground state (Fig. 4). In contrast, neither $CuH_2{}^+$ nor $AgH_2{}^+$ has a similar intermediate along the $^1A_1$ surface as shown in Fig. 6, although they both exhibit an inflection point corresponding to such a species. This difference is a result of the lanthanide contraction, which allows such *sd* hybridization to be particularly efficient for the third-row transition metals, as noted by Ohanessian *et al.*[58] Therefore, formation of an inserted intermediate, which can behave statistically, can occur for Au^+ but not for Cu^+ and Ag^+.

VI. CONCLUSION

Ground-state Au^+ ions are found to be more reactive with dihydrogen over a wide range of kinetic energies compared with the first-row and second-row group 11 transition metal cation systems. Analysis of the kinetic energy dependence of the reaction cross sections provides the BDE of Au^+–H, 2.13 ± 0.11 eV, which agrees well with quantum chemical calculations when performed using the B3LYP functional and the HW+/6-311++G(3df,3p) or Def2TZVPP basis sets. The bond of the AuH^+ ($^2\Sigma^+$) ground state is stronger than those of the other group 11 metal ions, Cu^+ and Ag^+, which is attributed to effective $6s\text{-}5d\sigma$ hybridization, a consequence of lanthanide contraction and relativistic effects.[58]

In the Au^+ system, calculations find that reactions with H_2 occur on a surface of singlet spin without barrier. The branching ratios observed in the Au^+ + HD reactions indicate that the ground state of Au^+ reacts with dihydrogen

largely via a direct mechanism, comparable to the behavior exhibited by the first and second row congeners, Cu^+ and Ag^+.[41,43] This can be rationalized using theoretical results, which show that the AuH_2^+ ($^1A_1$) ground state is an ion-induced dipole complex. However, because there is a low-lying insertion intermediate along the singlet ground state surface, the reactions of Au^+ with H_2 can also follow a more statistical pathway, leading to quantitative differences in the $\sigma_{MH+}/\sigma_{Total}$ branching ratio compared to the lighter congeners.

ACKNOWLEDGMENTS

This work is supported by the National Science Foundation.

[1]M. Haruta, N. Yamada, T. Kobayashi, and S. Iijima, J. Catal. **115**, 301 (1989).
[2]M. Haruta, Catal. Today **36**, 153 (1997).
[3]G. Bond and D. T. Thomson, Catal. Rev. Sci. Eng. **41**, 319 (1999).
[4]M. Haruta and M. Date, Appl. Catal. A **222**, 427 (2001).
[5]G. C. Bond, Catal. Today **72**, 5 (2002).
[6]A. Sanchez, S. Abbet, U. Heiz, W.-D. Schneider, H. Häkkinen, R. N. Barnett, and U. Landman, J. Phys. Chem. A **103**, 9573 (1999).
[7]H. Häkkinen and U. Landman, J. Am. Chem. Soc. **123**, 9704 (2001).
[8]T. M. Bernhardt, U. Heiz, and U. Landman, in *Nanocatalysis*, edited by U. Heiz and U. Landman (Springer-Verlag, Berlin, 2007).
[9]M. D. Hughes, Y.-J. Xu, P. Jenkins, P. McMorn, P. Landon, D. I. Enache, A. F. Carley, G. A. Attard, G. J. Hutchings, F. King, E. H. Stitt, P. Johnston, K. Griffin, and C. Kiely, Nature **437**, 1132 (2005).
[10]T. Fujitani, I. Nakamura, T. Akita, M. Okumura, and M. Haruta, Angew. Chem. Int. Ed. **48**, 9515 (2009).
[11]M. Boronat, F. Illas, and A. Corma, J. Phys. Chem. A **113**, 3750 (2009).
[12]D. M. Cox, R. Brickman, K. Creegan, and A. Kaldor, Z. Phys. D **19**, 353 (1991); D. M. Cox, R. Brickman, and K. A. Creegan, Mater. Res. Soc. Symp. Proc. **206**, 34 (1991).
[13]T. H. Lee and K. M. Ervin, J. Phys. Chem. **98**, 10023 (1994).
[14]B. E. Salisbury, W. T. Wallace, and R. L. Whetten, Chem. Phys. **262**, 131 (2000).
[15]J. Hagen, L. D. Socaciu, M. Elijazyfer, U. Heiz, T. M. Bernhardt, and L. Wöste, Phys. Chem. Chem. Phys. **4**, 1707 (2002).
[16]M. L. Kimble, A. W. Castleman, Jr., R. Mitric, C. Bűrgel, and V. Bonačić-KouteckÝ, J. Am. Chem. Soc. **126**, 2526 (2004).
[17]M. L. Kimble, N. A. Moore, G. E. Johnson, A. W. Castleman, Jr., C. Bürgel, R. Mitrić, and V. Bonačić-KouteckÝ, J. Chem. Phys. **125**, 204311 (2006).
[18]C. Bürgel, N. M. Reilly, G. E. Johnson, R. Mitrić, M. L. Kimble, A. W. Castleman, Jr., and V. Bonačić-KouteckÝ, J. Am. Chem. Soc. **130**, 1694 (2008).
[19]G. E. Johnson, N. M. Reilly, E. C. Tyo, and A. W. Castleman, Jr., J. Phys. Chem. C **112**, 9730 (2008).
[20]D. A. Weil and C. L. Wilkins, J. Am. Chem. Soc. **107**, 7316 (1985).
[21]A. K. Chowdhury and C. L. Wilkins, J. Am. Chem. Soc. **109**, 5336 (1987).
[22]R. Wesendrup, C. A. Schalley, D. Schroder, and H. Schwarz, Chem. Eur. J. **1**, 608 (1995).
[23]F.-X. Li, K. Gorham, and P. B. Armentrout, J. Phys. Chem. A **114**, 11043 (2010).
[24]F.-X. Li and P. B. Armentrout, J. Chem. Phys. **125**, 133114 (2006).
[25]R. H. Crabtree, *The Organometallic Chemistry of the Transition Metals*, 2nd ed. (Wiley, New York, 1994).
[26]G. A. Somorjai, *Introduction to Surface Chemistry and Catalysis* (Wiley, New York, 1994).
[27]P. B. Armentrout, ACS Symp. Ser. **428**, 18 (1990).
[28]P. B. Armentrout, Int. Rev. Phys. Chem. **9**, 115 (1990).
[29]P. B. Armentrout, J. Botero, in *Atomic and Molecular Processes in Fusion Edge Plasmas*, edited by R. K. Janev (Plenum, New York, 1995), pp. 433–460.
[30]P. B. Armentrout, in *Topics in Organometallic Chemistry*, edited by J. M. Brown and P. Hofmann (Springer-Verlag, Berlin, 1999), Vol. 4-I, p. 1.
[31]P. B. Armentrout and J. L. Beauchamp, Chem. Phys. **50**, 37 (1980).
[32]P. B. Armentrout and J. L. Beauchamp, J. Am. Chem. Soc. **103**, 784 (1981).
[33]P. B. Armentrout, L. F. Halle, and J. L. Beauchamp, J. Am. Chem. Soc. **103**, 962 (1981).
[34]P. B. Armentrout, L. F. Halle, and J. L. Beauchamp, J. Am. Chem. Soc. **103**, 6501 (1981).
[35]L. F. Halle, F. S. Klein, and J. L. Beauchamp, J. Am. Chem. Soc. **106**, 2543 (1984).
[36]M. A. Tolbert and J. L. Beauchamp, J. Am. Chem. Soc. **106**, 8117 (1984).
[37]J. L. Elkind and P. B. Armentrout, J. Chem. Phys. **84**, 4862 (1986).
[38]J. L. Elkind and P. B. Armentrout, Inorg. Chem. **25**, 1078 (1986).
[39]M. L. Mandich, L. F. Halle, and J. L. Beauchamp, J. Am. Chem. Soc. **106**, 4403 (1984).
[40]J. L. Elkind and P. B. Armentrout, J. Phys. Chem. **91**, 2037 (1987).
[41]J. L. Elkind and P. B. Armentrout, J. Phys. Chem. **90**, 6576 (1986).
[42]J. L. Elkind, L. S. Sunderlin, and P. B. Armentrout, J. Phys. Chem. **93**, 3151 (1989).
[43]Y.-M. Chen, J. L. Elkind, and P. B. Armentrout, J. Phys. Chem. **99**, 10438 (1995).
[44]M. R. Sievers, Y.-M. Chen, and P. B. Armentrout, J. Phys. Chem. **100**, 54 (1996).
[45]X.-G. Zhang, C. Rue, S.-Y. Shin, and P. B. Armentrout, J. Chem. Phys. **116**, 5574 (2002).
[46]X.-G. Zhang and P. B. Armentrout, J. Chem. Phys. **116**, 5565 (2002).
[47]F.-X. Li, X.-G. Zhang, and P. B. Armentrout, J. Phys. Chem. B **109**, 8350 (2005).
[48]P. B. Armentrout and F.-X. Li, J. Chem. Phys. **121**, 248 (2004).
[49]P. B. Armentrout, R. V. Hodges, and J. L. Beauchamp, J. Chem. Phys. **66**, 4683 (1977).
[50]P. B. Armentrout, R. V. Hodges, and J. L. Beauchamp, J. Am. Chem. Soc. **99**, 3163 (1977).
[51]P. B. Armentrout and J. L. Beauchamp, Chem. Phys. **48**, 315 (1980).
[52]R. Georgiadis and P. B. Armentrout, J. Phys. Chem. **92**, 7060 (1988).
[53]N. F. Dalleska, K. C. Crellin, and P. B. Armentrout, J. Phys. Chem. **97**, 3123 (1993).
[54]P. B. Armentrout and B. L. Kickel, in *Organometallic Ion Chemistry*, edited by B. S. Freiser (Kluwer, Dordrecht, 1996), p. 1.
[55]P. B. Armentrout, Int. J. Mass Spectrom. **200**, 219 (2000).
[56]P. B. Armentrout, J. Am. Soc. Mass Spectrom. **13**, 419 (2002).
[57]P. B. Armentrout, *Modern Mass Spectrometry*, Topics in Current Chemistry Vol. 225, edited by C. Schalley (Springer-Verlag, Berlin, 2003), pp. 233–262.
[58]G. Ohanessian, M. J. Brusich, and W. A. Goddard III, J. Am. Chem. Soc. **112**, 7179 (1990).
[59]P. Schwerdtfeger, M. Dolg, W. H. E. Schwarz, G. A. Bowmaker, and P. D. W. Boyd, J. Chem. Phys. **91**, 1762 (1989).
[60]Y. Ishikawa, G. L. Malli, and N. C. Pyper, Chem. Phys. Lett. **194**, 481 (1992).
[61]U. Kaldor and B. A. Hess, Chem. Phys. Lett. **230**, 1 (2002).
[62]J. Hrušák, R. H. Hertwig, D. Schröder, P. Schwerdtfeger, W. Koch, and H. Schwarz, Organometallics **14**, 1284 (1995).
[63]S. K. Loh, D. A. Hales, L. Lian, and P. B. Armentrout, J. Chem. Phys. **90**, 5466 (1989).
[64]E. Teloy and D. Gerlich, Chem. Phys. **4**, 417 (1974).
[65]D. Gerlich, Adv. Chem. Phys. **82**, 1 (1992).
[66]K. M. Ervin and P. B. Armentrout, J. Chem. Phys. **83**, 166 (1985).
[67]P. J. Chantry, J. Chem. Phys. **55**, 2746 (1971).
[68]R. H. Schultz and P. B. Armentrout, Int. J. Mass Spectrom. Ion Process. **107**, 29 (1991).
[69]W. J. Chesnavich and M. T. Bowers, J. Phys. Chem. **83**, 900 (1979).
[70]N. Aristov and P. B. Armentrout, J. Am. Chem. Soc. **108**, 1806 (1986).
[71]P. B. Armentrout, in *Advances in Gas Phase Metal Ion Chemistry*, edited by N. G. Adams and L. M. Babcock (JAI, Greenwich, 1992), Vol. 1, p. 83.
[72]K. P. Huber and G. Herzberg, *Molecular Spectra and Molecular Structure* (Van Nostrand Reinhold, New York, 1979), Vol. IV.
[73]M. J. Frisch, G. W. Trucks, H. B. Schlegel *et al.*, GAUSSIAN 03, Revision B.02 (2003) Gaussian, Inc., Pittsburgh, PA.
[74]M. Rosberg and J.-F. Wyart, Phys. Scr. **55**, 690 (1997).
[75]C. M. Brown and M. L. Ginter, J. Opt. Soc. Am. **68**, 243 (1978).
[76]S. Smoes, F. Mandy, A. Vander Auwera-Mahieu, and J. Drowart, Bull Soc. Chim. Belges **81**, 45 (1972).
[77]J. B. Pedley and E. M. Marshall, J. Phys. Chem. Ref. Data **12**, 967 (1983).
[78]A. D. Becke, J. Chem. Phys. **98**, 5648 (1993).

[79]C. Lee, W. Yang, and R. G. Parr, Phys. Rev. B. **37**, 785 (1988).
[80]P. J. Hay and W. R. Wadt, J. Chem. Phys. **82**, 299 (1985).
[81]M. Dolg, H. Stoll, H. Preuss, and R. M. Pitzer, J. Phys. Chem. **97**, 5852 (1993).
[82]W. J. Stevens, M. Krauss, H. Basch, and P. G. Jasien, Can. J. Chem. **70**, 612 (1992).
[83]F. Weigend and R. Ahlrichs, Phys. Chem. Chem. Phys. **7**, 3297 (2005).
[84]S. A. Varganov, R. M. Olson, M. S. Gordon, and H. Metiu, J. Chem. Phys. **119**, 2531 (2003).
[85]M. C. Holthausen, C. Heinemann, H. H. Cornehl, W. Koch, and H. Schwarz, J. Chem. Phys. **102**, 4931 (1995).
[86]J. L. Elkind and P. B. Armentrout, J. Phys. Chem. **89**, 5626 (1985).
[87]P. B. Armentrout, in *Gas Phase Inorganic Chemistry*, edited by D. H. Russell (Plenum, New York, 1989), p. 1.
[88]P. B. Armentrout, in *Selective Hydrocarbon Activation: Principles and Progress*, edited by J. A. Davies, P. L. Watson, A. Greenberg, and J. F. Liebman (VCH, New York, 1990), p. 467.
[89]M. E. Weber, J. L. Elkind, and P. B. Armentrout, J. Chem. Phys. **84**, 1521 (1986).
[90]Z. J. Wu, J. Phys. Chem. A **109**, 5951 (2005).
[91]L. S. Sunderlin, N. Aristov, and P. B. Armentrout, J. Am. Chem. Soc. **109**, 78 (1987).
[92]J. D. Burley, K. M. Ervin, and P. B. Armentrout, Int. J. Mass Spectrom. Ion Process. **80**, 153 (1987).
[93]P. B. Armentrout, ACS Symp. Ser. **502**, 194 (1992).